# Graphical Abstract

**Thermal transport in planar $sp^2$-hybridized carbon allotropes: A comparative study of biphenylene network, pentaheptite and graphene**

Penghua Ying, Ting Liang, Yao Du, Jin Zhang, Qiangqiang Ma, Xiaoliang Zeng, Zheng Zhong

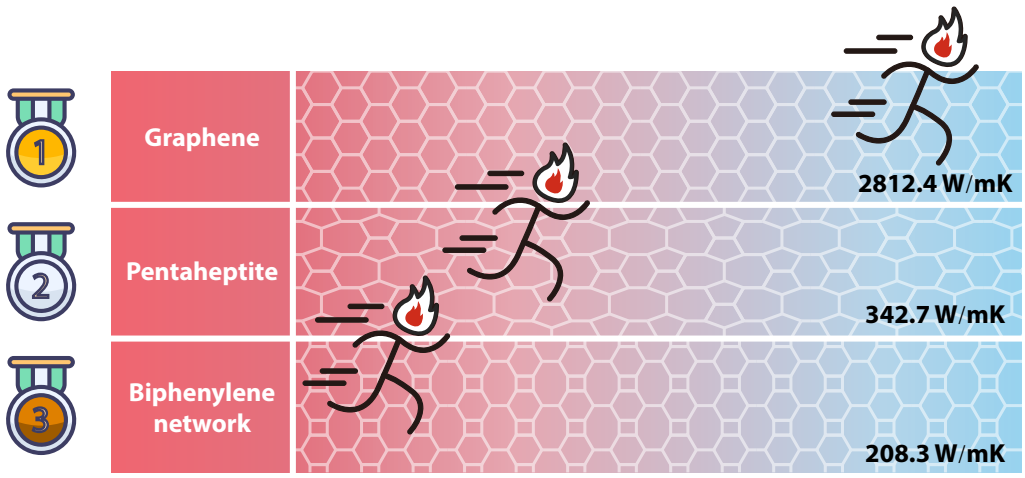

# Highlights

**Thermal transport in planar $sp^2$-hybridized carbon allotropes: A comparative study of biphenylene network, pentaheptite and graphene**

Penghua Ying, Ting Liang, Yao Du, Jin Zhang, Qiangqiang Ma, Xiaoliang Zeng, Zheng Zhong

- Thermal transport properties of three carbon allotropes are investigated by three MD-based methods including HNEMD, EMD, and NEMD.
- Thermal conductivity of biphenylene network only corresponds to about one-thirteenth of graphene.
- The great reduction in thermal conductivity of biphenylene network and pentaheptite arise from the decline of structural symmetry.
- The analysis of phonon mean free path, phonon group velocity, elastic modulus together with electron localization function are performed to reveal the mechanism.

# Thermal transport in planar $sp^2$-hybridized carbon allotropes: A comparative study of biphenylene network, pentaheptite and graphene

Penghua Ying[a,1], Ting Liang[b,1], Yao Du[a,1], Jin Zhang[a,**], Qiangqiang Ma[b], Xiaoliang Zeng[b], Zheng Zhong[a,*]

[a]*School of Science, Harbin Institute of Technology, Shenzhen, 518055, PR China*
[b]*Shenzhen Institute of Advanced Electronic Materials, Shenzhen Institute of Advanced Technology, Chinese Academy of Sciences, Shenzhen, 518055, PR China*

**Abstract**

The biphenylene network with periodically arranged four-, six-, and eight-membered rings has been successfully synthesized in very recent experiments. This novel two-dimensional (2D) carbon allotrope has potentials in applications of lithium storage and carbon-based circuitry. Understanding the thermal transport property of biphenylene network is of critical importance for the performance and reliability of its practice applications. To this end, the thermal transport in biphenylene network is comprehensively investigated in this paper with the aid of homogeneous non-equilibrium molecular dynamics (HNEMD), equilibrium molecular dynamics (EMD) and nonequilibrium molecular dynamics (NEMD) simulations. For the sake of comparison, the thermal conductivity of some other 2D $sp^2$-hybridized carbon allotropes such as graphene and pentaheptite is also investigated using the same methods. The thermal conductivities of biphenylene network and pentaheptite predicted from the HNEMD method are, 208.3 W/(mK) and 342.7 W/(mK), respectively, which only equal to one-thirteenth and one-eighth of the value (2812.4 W/(mK)) of graphene. These results obtained from the HNEMD method are found to be in good agreements with the results extracted from EMD and NEMD methods, indicating the reliability of the present results.

*Corresponding author
**Corresponding author
*Email addresses:* jinzhang@hit.edu.cn (Jin Zhang), zhongzheng@hit.edu.cn (Zheng Zhong)
[1]These authors contributed equally.

Based on the spectral heat current decomposition method, the thermal conductivity of all three 2D carbon allotropes is found to be mainly attributed to the flexural phonon mode. Through the analysis of phonon property, mechanical property and electron density distribution, the low thermal conductivity of biphenylene network and pentaheptite smaller than that of graphene is found to stem from the decline in their structural symmetry, which leads to the aggravation of phonon scattering, the decrease of phonon group velocity and the reduction of phonon mean free path.

*Keywords:* biphenylene network, planar carbon allotropes, thermal conductivity, molecular dynamics, phonon transport

## 1. Introduction

Since Geim and Novoselov experimentally discovered graphene by using micromechanical cleavage in 2004 [1], this two-dimensional (2D) carbon allotrope has attracted a great number of interest in academia and industry by virtue of its superior and novel physical properties. For example, experiments demonstrate that graphene has an ultrahigh strength of 130 GPa, a large Young's modulus up to 1 TPa [2], and an extremely high thermal conductivity in the range of 3000-5800 W/(mK) [3–6]. Inspired by the extraordinary structural and material properties observed in graphene, numerous 2D materials based on other elements have also been reported, such as hexagonal boron nitride, transitional metal dichalogenides (e.g., $MoS_2$ and $MoTe_2$), and many monoelements including silicene, germanene, phosphorene, stanene and borophene [7]. In addition, the demand of other 2D carbon allotropes has also stimulated substantial efforts in searching pure-carbon nanodevices beyond graphene [8]. To date, a large amount of novel 2D carbon allotropes have been theoretically predicted with the aid of the structure searching method and first-principles calculations [9–16], though only a few have been successfully synthesized in experiments. In 2010, graphdiyne whose crystal lattice is arranged with sp and $sp^2$-bonded carbon atoms was reported by Li and coworkers in their experimental study [17]. Very recently, motivated by previous works [18, 19], Fan and coworkers synthesized the biphenylene network in experiments [20], which can be treated as the second pure $sp^2$-hybridized carbon allotropes with repeating nonhexagonal motifs along both planar dimensions. These biphenylene networks are reported to have the application potentials in lithium storage and carbon-based circuitry.

Understanding the thermal transport in 2D carbon allotropes not only provides an important guidance for their thermal management applications in nanodevices, but also is the essential step to reveal the fundamental mechanism of phonon transport in low-dimensional systems. Theoretically, the lattice thermal conductivity of a crystal can be obtained by lattice dynamic methods or molecular dynamics (MD)-based methods. By using the homogeneous non-equilibrium molecular dynamics (HNEMD) method [21], the thermal conductivity of graphene was predicted to be around 3000 W/(mK) at room temperature, which is higher than any other known 2D carbon allotropes. The outstanding thermal transport property observed in graphene can be attribute to its strong $sp^2$-hybridized bond and planar honeycomb lattice with very high symmetry. As for other 2D carbon allotropes, their thermal conductivity is reported to be substantially smaller than that of graphene. For example, based on phonon Boltzmann transport equation and first-principle calculations, the thermal conductivities of $\alpha$, $\beta$, and $\gamma$ graphyne with sp and $sp^2$-hybridized bonds were predicted to be 21.1, 22.3 and 106.2 W/(mK) at room temperature, respectively, which are one order or two orders of magnitude smaller than 2962.8 W/(mK) of graphene [22]. Using the same method, the thermal conductivity of penta-graphene [23] with sp and $sp^3$-hybridized bonds was predicted to be 645 W/(mK) at room temperature [24], which is also significantly smaller than that of graphene. Equilibrium molecular dynamics (EMD) simulations together with Green-Kubo method [25, 26] were employed to predict the thermal conductivities of OPG-L and OPG-Z [27] with pure $sp^2$-hybridized bonds, which are 313-344 W/(mK) and 233-261 W/(mK) at room temperature, respectively. Very recently, by extrapolating the non-equilibrium molecular dynamics (NEMD) results [28], the thermal conductivities of penta-graphene (392 W/(mK)) and three pure $sp^2$-hybridized 2D carbon allotropes including $\psi$-graphene [29] (338 W/(mK)), pop-graphene [30] (156.5 W/(mK)), and net-W [19] (156.5 W/(mK)) were obtained. All existing results suggest a big difference between graphene and other carbon allotropes.

Compared with a large number of studies reported for the thermal conductivity of graphene [31–35], the study on the thermal transport in some other 2D carbon allotropes is stills in its infancy stage. Especially, the newly synthesized biphenylene network [20] and the theoretically predicted pentaheptite [10] show a periodically arranged nonbenzenoid structure different from pristine honeycomb lattice in graphene. This lattice structure difference should make biphenylene network and pentaheptite have a thermal

transport property different from that of graphene. Thus, it is essential to conduct a comprehensive study on the thermal conductivity of these new $sp^2$-hybridized 2D carbon allotropes. In this work, a comparative study on the thermal transport in planar $sp^2$-hybridized carbon allotropes including graphene, biphenylene network, and pentaheptite is performed by using graphics processing units molecular dynamics (GPUMD) [36] simulations. Three MD-based methods including HNEMD, EMD, and NEMD are used to predict the thermal conductivity of carbon allotropes. The spectral heat current (SHC) analysis, lattice dynamics calculations, electron localization function calculations and tensile simulations are also performed to reveal the mechanism underlying the phonon transport in these carbon allotropes.

## 2. Model and Methods

### *2.1. Simulation Model*

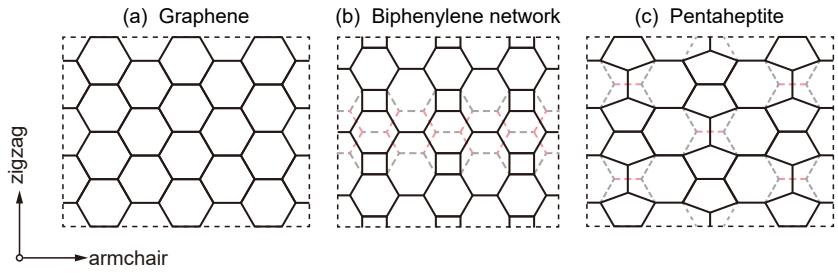


Figure 1: Lattice structures of three planar carbon allotropes including (a) graphene, (b) biphenylene network with four-, six-, and eight-membered carbon rings, and (c) pentaheptite with five- and seven-membered carbon rings.

As shown in Figure 1, the lattice structures of biphenylene network and pentaheptite considered here can be constructed by reorganizing some partial bonds in graphene. Specifically, when generating pentaheptite, all six-membered carbon rings (i.e., rings of carbon atoms) in graphene are equally split into five- and seven- membered carbon rings. In generating the biphenylene network, partial six-membered rings in graphene are split into four- and eight- membered carbon rings, resulting in the coexistence of ternary (four-, six-, and eight-membered) rings in the materials. Here, the cell size of graphene, biphenylene network and pentaheptite is set as 25 nm $\times$ 25 nm in all HNEMD and EMD simulations, which is sufficiently large to eliminate the finite-size effect [21, 34]. Correspondingly, there are 24072, 22110, and 24072

atoms in the present simulation models of graphene, biphenylene network, and pentaheptite, respectively. Periodic boundary conditions are applied in both planar directions, while the free boundary condition is applied in the out-of-plane direction. It is noted that the principle directions, i.e., armchair and zigzag directions in pentaheptite and biphenylene are defined as the same as those in graphene. In other words, the definition of the armchair and zigzag directions of biphenylene network and pentaheptite is unchanged during the structural construction based on graphene (see dotted lines in Figure 1(b-c)).

### *2.2. Thermal Conductivity Calculations*

All calculations of thermal conductivity based on MD simulations were performed at room temperature (300 K) using the open source GPUMD package [36], in which the standard Newton equations of motion are integrated in time by the velocity-Verlet integration algorithm [37]. By the virtue of powerful GPUs, GPUMD is of higher efficiency in calculating thermal conductivity of nanomaterials when compared to any other MD codes such as LAMMPS [38]. In addition, GPUMD can correctly calculate the heat flux of multi-body potential systems, which is significantly underestimated by LAMMPS [39–41]. The time steps in the simulations of graphene, biphenylene network, and pentaheptite were set as 0.5 fs, 0.25 fs, and 0.1 fs, respectively. The thermal conductivities in two principle directions including both armchair and zigzag directions were considered for all carbon allotropes. The optimized Tersoff force field [42] was employed to describe the atomic interactions in all planar carbon allotropes considered here. The optimized Tersoff force field has been widely utilized in previous MD simulations on the mechanical and thermal properties of various carbon-based 2D materials such as graphene [32, 35, 43–46], penta-graphene [47, 48], hexagonal boron nitride [49, 50], $C_3N$ [51, 52], $BC_3N$, $BC_6N$ [53] and so on. To examine the reliability of this force field in describing the 2D carbon allotropes considered here, we compared the lattice lengths and energies of these 2D carbon allotropes predicted from the optimized Tersoff force field to the results calculated from first-principle calculations (see Figure S1 in supplementary materials). It was found that the results obtained from these two methods agree very well with each other. Specifically, the energies of biphenylene network and pentaheptite obtained from the optimized Tersoff potential are 0.37 eV/atom and 0.70 eV/atom higher than that of graphene, respectively, which are consistent with the corresponding results of 0.24 eV/atom and 0.47 eV/atom

obtained from first-principles calculations. The energy of both biphenylene network and pentaheptite is higher than that of graphene. As for the newly synthesized biphenylene network, we also compared its phonon dispersion relations calculated from various force fields including aforementioned optimized Tersoff, airebo [54], and ReaxFF[55] to the results extracted from first-principle calculations (see Figure S2 in supplementary materials). It was demonstrated that among these three force fields, the optimized Tersoff force field has the most accuracy in describing the phonon band structure of biphenylene network.

In this work, the thermal conductivity of planar carbon allotropes was calculated by three different MD-based methods including HNEMD, EMD, and NEMD. The corresponding theory and simulation details of these methods were briefly introduced below.

*2.2.1. HNEMD Simulations*

Based on the non-canonical linear response theory, Evans proposed the HNEMD method in 1982 [56], which was recently extended to generalized many-body potentials in GPUMD package developed by Fan and coworkers [21]. The HNEMD method has been widely applied in calculating the thermal conductivity of various 2D materials such as graphene [21, 57], polyaniline ($C_3N$) [52], $MoS_2$ [58], and etc. For planar carbon allotropes considered here, the thermal conductivity along armchair or zigzag direction is given by

$$k(t) = \frac{1}{t}\int_0^t \frac{\langle J_q(\tau)\rangle}{TVF_e}\mathrm{d}\tau, \tag{1}$$

where $t$, $V$, and $T$ are, respectively, the production time, system volume, and temperature. $\langle J_q(\tau)\rangle$ is the nonequilibrium heat current induced by the driving force $F_e$. The symbol $\langle\rangle$ denotes the average over simulation time $t$. The volume of 2D materials usually depends on their thickness, which has diverse theoretical predictions in various literatures [59]. To avoid the influence of thickness definition and, meanwhile, facilitate the comparison among three carbon allotropes considered here, a conventional value of 0.335 nm is used here as the thickness for all three carbon allotropes. Previous studies demonstrated that the driving force parameter $F_e$ should be within a reasonable range. On one hand, $F_e$ has to be small enough to keep the system within the linear-response regime and converge within the simulation time. On the other hand, $F_e$ has to be large enough to obtain a reliable result with a large signal-to-noise ratio [56, 60, 61]. According to the rule of

thumb developed by Mandadapu and coworkers [60], the value of $F_e$ should be roughly smaller than $1/\lambda_{max}$, where $\lambda_{max}$ denotes the maximum phonon mean-free-path (MFP). As shown in Figure 2 (a-b), taking the biphenylene network as an example, we tested the sensitivity of $k(t)$ to the parameter $F_e$. The value of $k(t)$ is found to diverge with increasing $t$ when $F_e \geq 0.6$ $\mu\text{m}^{-1}$. The convergence of $k(t)$ is found at $F_e \leq 0.5$ $\mu\text{m}^{-1}$. However, a very small value 0.05 $\mu\text{m}^{-1}$ of $F_e$ results in a significant noise. Under this circumstance, more simulations are needed to obtain a more reliable value of $k(t)$. Based on the above analyses, $F_e = 0.1$ $\mu\text{m}^{-1}$ was applied for all carbon allotropes considered in this work, which is consistent with the value selected in the previous HNEMD simulations of graphene and polyaniline ($C_3N$) [21, 52].

Energy minimization was performed to the initially constructed models of all carbon allotropes to obtain their equilibrium configurations. In doing this, the samples were relaxed in the NPT ensemble (constant number of particles, pressure, and temperature) with zero pressure and, subsequently, in the NVT ensemble (constant number of particles, volume, and temperature) for 100 ps. A total time of 10 ns was used to obtain the converged $k$, and the raw data of thermal conductivity was averaged for each 1 ps. For each calculation of the thermal conductivity, eight independent HNEMD simulations were performed (see Figures 2 and 3), corresponding to a total production time of 80 ns. Finally, the averaged result of these eight simulations at $t = 10$ ns was taken as the values of $k$.

*2.2.2. EMD Simulations*

On the basis of fluctuation-dissipation theorem [62], we also calculated the thermal conductivity of planar carbon allotropes by EMD simulations together with Green-Kubo method [25, 26]. As shown below, this method calculates the running thermal conductivity $k(t)$ by integrating heat current autocorrelation function (HCACF) over a given correlation time $t$

$$k(t) = \frac{V}{k_B T^2} \int_0^t \langle J(0)J(\tau)\rangle \, \mathrm{d}\tau, \tag{2}$$

where $k_B$ is Boltzmann's constant and $\langle J(0)J(\tau)\rangle$ is the average HCACF over different time origins with $J$ being the heat current.

It is worth noting that the HNEMD method and EMD method are physically equivalent to each other. However, due to the introduction of the fictitious driving force in a fixed direction to the system, the HNEMD method enjoys much higher computational efficiency and larger signal-to-noise ratio

[21]. Therefore, compared with the HNEMD method, the EMD method requires more independent simulations to obtain a reliable result. As shown in Fig. 4, we carried out 80 independent simulations and each simulation has a correlation time of 2 ns. The obtained 80 results were averaged to obtain the converged running thermal conductivity. All other simulation parameters in the present EMD simulations are the same as those set in the above HNEMD simulations. For each EMD simulation, the production time is 20 ns that is 10 times as long as the correlation time. Each EMD result was obtained by using a total production time of 1600 ns. For all carbon allotropes, the averaged $k(t)$ converges well in the time ranging from 1 ns to 2ns. The final value of $k$ obtained from EMD method was obtained by averaging the results in the last 500 ps. In addition, as for $k$ obtained from both HNEMD and EMD methods, the corresponding standard statistical error $\sigma_n$ is calculated as

$$\sigma_n = \frac{\sqrt{\sum_{i=1}^{n}(k_i - \bar{k})^2}}{n}, \tag{3}$$

where $n$ is the number of independent simulations and $\bar{k}$ is the averaged thermal conductivity.

*2.2.3. NEMD Simulations*

Both the aforementioned HNEMD and EMD methods are homogeneous methods. Thus, the size effect in them is usually extremely small, which can be generally ignored. To study the thermal transport in finite-sized carbon allotropes with a length of $L$, we calculated the thermal conductivity $k$ by NEMD simulations using the following formula

$$k(L) = \frac{Q/S}{\Delta T/L}, \tag{4}$$

where $Q$, $\Delta T$, and $L$ are the the energy transfer rate, temperature difference, and effective length between the heat source and heat sink. In Eq. 4, $S$ is the area of the cross section perpendicular to the transport direction. Li and coworkers [46] indicated that the nonlinear part of the temperature profile extracted from NEMD simulations should be considered in the calculation of the thermal conductivity. In other words, the temperature gradient should be calculated directly as $\Delta T/L$ here instead of the slope of the linear region of the temperature profile away from the local thermostats.

Fig 5(a) shows the setup of NEMD simulations performed in this study. The system along the thermal transport direction, i.e., heat flux direction was divided into three parts, which include the fixed regions with the same length at two ends, two thermostats (the heat source and heat sink regions) with the same length adjacent to the fixed regions, and the thermal transport region between heat source and heat sink. Herein, the lengths of fixed regions and thermostats were set as 1 nm and 25 nm, respectively. The dimension of the sample perpendicular to the heat flux direction was set as 25 nm. Correspondingly, $S$ of all samples in NEMD simulations is 8.375nm$^2$ with a conventional thickness of 0.335 nm being selected here. As shown in Fig 5(b), five different lengths ranging from 25nm to 200nm were considered for all samples in simulations. Each NEMD simulation was performed for 6 ns, in which the stable temperature distribution was achieved within the initial 1 ns, while the temperature gradient was obtained by averaging over the final 5 ns.

### *2.3. Spectral Heat Current Analysis*

Based on the NEMD and HNEMD results, the spectral heat current (SHC) analyses were further conducted to obtain the frequency-dependent MFP and length-dependent thermal conductivity. Firstly, the thermal conductivity calculated from the HNEMD method (see Eq. 1) can be spectrally decomposed in the frequency domain as follows: [18, 21, 32, 63, 64]

$$k(\omega) = \frac{2\widetilde{K}\omega}{TVF_e}. \tag{5}$$

Here, $\widetilde{K}\omega$ is the Fourier transform of the virial-velocity correlation function, which can be defined as [64]:

$$K(t) = \sum_i W_i(0) \cdot v_i(t), \tag{6}$$

where $W_i$ and $v_i$ denote the virial tensor and velocity of atom $i$, respectively. Secondly, the quasi-ballistic spectral thermal conductance $G(\omega)$ based on the NEMD results can be similarly obtained. Finally, the frequency-dependent MFP $\lambda(\omega)$ can be obtained from $K(\omega)$ and $G(\omega)$ as follows:

$$\lambda(\omega) = K(\omega)/G(\omega). \tag{7}$$

The length-dependent $k(L)$ can be expressed as the following classical first-order extrapolation formula: [65]

$$k(L) = \frac{k_\infty}{1 + \lambda_\infty / L}, \tag{8}$$

where $k_\infty$ is the length-independent thermal conductivity at $1/L = 0$, and $\lambda_\infty$ is the phonon MFP for the infinite system. Further, $k(L)$ can be obtained by integrating Eq. 8 in the frequency domain:

$$k(L) = \int \frac{k_\omega}{1 + \lambda_\omega / L} \frac{d\omega}{2\pi}. \tag{9}$$

Based on Eqs. 5 and 6, we obtained the HNEMD-based SHC result and NEMD-based SHC result, respectively. Based on Eqs. 7 and 9, we obtained the frequency-dependent MFP and length-dependent thermal conductivity of carbon allotropes, respectively.

### *2.4. First-principles Calculations*

First-principles calculations were conducted here to predict the lattice length, phonon dispersion relations, and electron localization function of planar carbon allotropes. All first-principles calculations were based on the Vienna Ab-initio Simulation Package (VASP) [66–68] together with the generalized gradient approximation (GGA) of the Perdew-Burke-Ernzerhof functional form (PBE) for the exchange-correlation potential [69]. For the sake of comparison, we used the 2D Bravais lattices with rectangular symmetry for all three carbon allotropes as shown in the inset of Fig. S1. The periodic boundary conditions were applied along all three Cartesian directions. A vacuum layer of 10 $\mathring{A}$ was set to avoid adjacent image-image interactions along the thickness directions. The convergence condition for the electronic self consistence loop was set as the total energy change smaller than $10^{-7}$eV. The Monkhorst-Pack k-point mesh sizes for graphene, biphenylene network, and pentaheptite were set as $15 \times 9 \times 1$, $9 \times 8 \times 1$, and $6 \times 4 \times 1$, respectively.

The structural optimization was performed by conjugate gradient method with the convergence condition for the ionic relaxation loop being the Hellmann Feynman forces smaller than 0.001 eV/Å. The second-order (harmonic) interatomic force constants were calculated by the density functional perturbation theory (DFPT) methods. First-principles-based phonon dispersion relations and the corresponding group velocities were obtained by the

PHONOPY package [70] with inputs provided by the DFPT results. For the sake of comparison, the high symmetry directions of the first Brillouin zone were set as $\Gamma - \mathrm{X} - \mathrm{S} - \mathrm{Y} - \Gamma$ for all carbon allotropes (see Figs. S1 and 8). The VESTA package [71] was used to illustrate charge densities, while the VASPKIT package [72] was used to prepare parts of the input file for first-principle calculations.

## 3. Results and Discussion

### *3.1. Thermal Conductivity of Planar Carbon Allotropes*

In this section, we study the thermal conductivity of three planar carbon allotropes including graphene, biphenylene network, and pentaheptite using HNEMD, EMD, and NEMD. The thermal conductivities calculated by these three methods are cross-checked with each other. Efforts are also made to compare the thermal transport properties of these carbon allotropes including the magnitude of thermal conductivity, the anisotropy of thermal conductivity, and the corresponding contributions of in-plane and out-of-plane phonon modes.

We first investigate the thermal transport property of biphenylene network using HNEMD simulations. The thermal conductivities along armchair and zigzag directions are denoted as $k_{arm}$ and $k_{zig}$, respectively, which are obtained from Eq. (1) by applying the the driving force along the same direction. As shown in Fig. 2(c-d), $k_{arm}$ and $k_{zig}$ are $213.1 \pm 3.5$ W/(mK) and $203.5 \pm 5.8$ W/(mK), respectively, indicating a very trivial anisotropy of the thermal transport property existing in the biphenylene network. Following the heat current decomposition method proposed by Fan and coworkers [32], we decompose $k$ into the in-plane and out-of-plane directions, the components of which are $k_{\mathrm{in}}$ and $k_{\mathrm{out}}$, respectively. These two components correspond to the contribution of in-plane and out-of-plane (flexural) phonon branches, respectively. The thermal conductivities in the armchair and zigzag directions are averaged and similarly decomposed into $k_{\mathrm{in}}$ and $k_{\mathrm{out}}$. The results of $k_{\mathrm{in}}$ and $k_{\mathrm{out}}$ are 38.1 W/(mK) and 170.2 W/(mK), respectively, which indicates that the flexural component contributes dominantly (about four-fifths) to the thermal transport in biphenylene network. In addition, it is also found that in both directions $k_{\mathrm{in}}$ converges shortly at $t = 4$ ns, which is much faster than $k_{\mathrm{out}}$ converging at $t = 8$ ns.

Figure 3 shows the running thermal conductivity of pentaheptite and graphene calculated through the HNEMD method. The values of $k_{arm}$ and

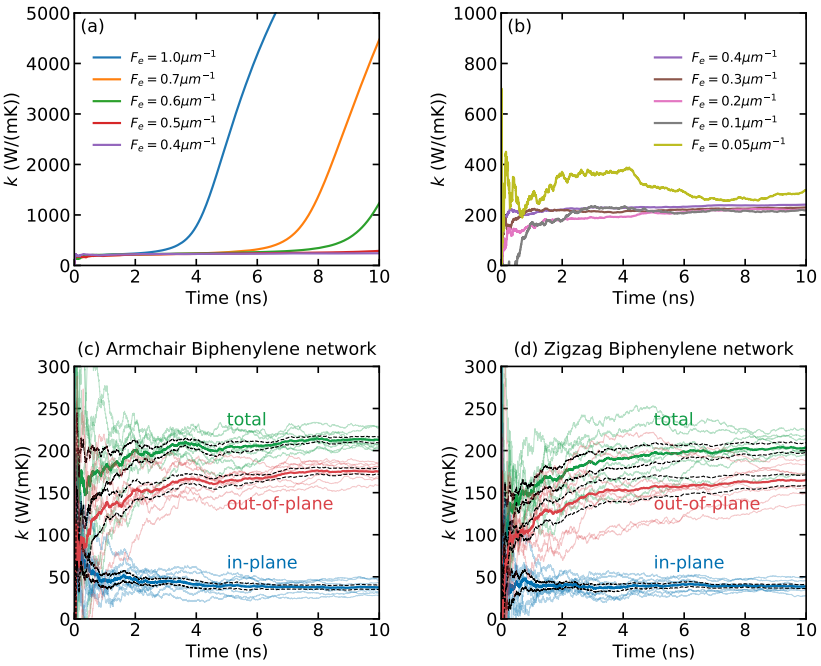


Figure 2: Thermal conductivity of biphenylene network with a szie of 25 nm × 25 nm, which is calculated by HNEMD method at 300 K. (a-b) Results of the running thermal conductivity when $F_e$ ranges from 0.05 $\mu$m$^{-1}$ to 1.0 $\mu$m$^{-1}$. (c-d) Thermal conductivity of biphenylene network along armchair and zigzag directions, respectively. The total thermal conductivity is decomposed into an in-plane component and an out-of-plane component. Each production thermal conductivity (see solid lines) is obtained by averaging by eight independent simulations (see semi-transparent lines).

$k_{zig}$ of pentaheptite are 362.9 ± 8.5 W/(mK) and 322.4 ± 9.3 W/(mK), respectively, while the values of $k_{arm}$ and $k_{zig}$ of graphene are 2807.3 ± 11.0 W/(mK) and 2817.5 ± 18.0 W/(mK), respectively. The thermal conductivity of graphene calculated here is in good agreement with the previous studies based on HNEMD simulations such as 2847 ± 49.0 W/(mK) in Ref. [21] and 2900 ± 100.0 W/(mK) in Ref. [32]. Table 1 shows a comparison of $k_{arm}$ and $k_{zig}$ among all three carbon allotropes. It is clearly found that the anisotropy of the thermal conductivity of biphylene network and graphene is very trivial. However, as for pentaheptite, its $k_{arm}$ of 362.9 W/(mK) is larger than its $k_{zig}$ having a value of 322.4 W/(mK). This result suggests that pentaheptite possesses a larger thermal conductivity in the armchair direction. For the sake of comparison, we herein also calculate the scalar

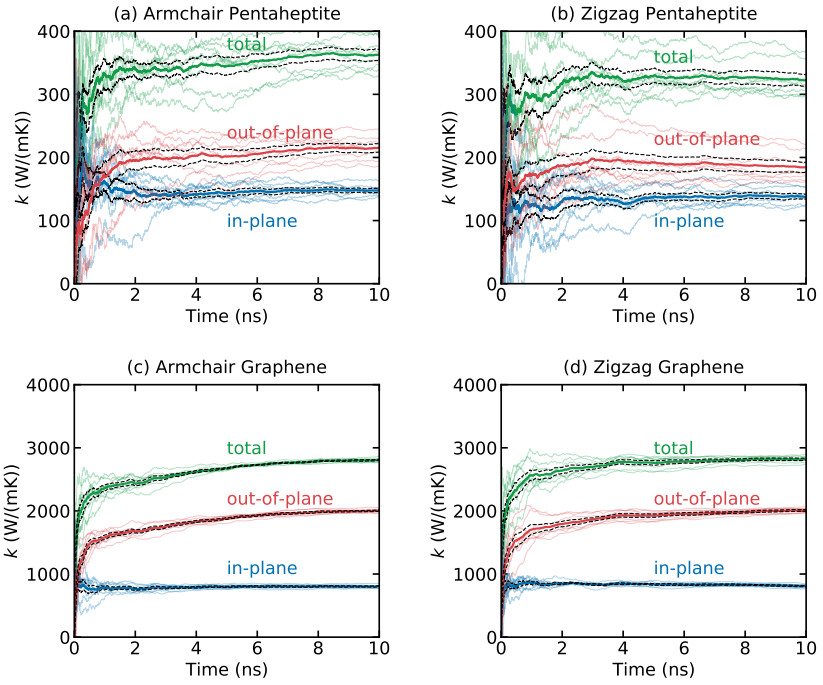


Figure 3: Thermal conductivity along armchair and zigzag directions of (a and b) pentahepitite and (c and d) graphene with a size of 25 nm × 25 nm, which is calculated by HNEMD method at 300 K. The total thermal conductivity is decomposed into an in-plane component and an out-of-plane component. Each final thermal conductivity (see solid lines) is obtained by averaging eight independent simulations (see semi-transparent lines).

thermal conductivity $k$ for each carbon allotrope, which has the definition of $k = (k_{arm} + k_{zig})/2$. By comparing three carbon allotropes as listed in Table 1, we find that $k$ of both biphenylene network and pentaheptite is much lower than that of graphene. Specifically, values of $k$ of both biphenylene network and pentaheptite are, respectively, only about one-thirteens and one-eights of the value of graphene. In addition, it is also found that the flexural component contributes about two-thirds of the total thermal conductivity of both graphene and pentaheptite. $k_{in}$ of biphenylene network having the values of 38.1 W/(mK) is much lower than 142.8 W/(mK) of pentaheptite, which results in a much lower value of $k$ (208.3 W/(mK)) in biphenylene network as compared to the value of 342.7 W/(mK) in pentaheptite.

The thermal conductivity of biphenylene network (208.3 W/(mK)) and pentaheptite (342.7 W/(mK)) calculated here is close to the value of 233-344

W/(mK) reported for other carbon allotropes with five-five-eight-membered rings [48], but is significantly smaller than 2013 W/(mK) of graphene-like $C_3N$ [52]) and 656 W/(mK) of hexagonal boron nitride[49]. This finding indicates that the symmetry breaking of the pristine honeycomb lattice during the structural construction of carbon allotropes with hybrid-membered rings such as biphenylene network and pentaheptite from graphene can cause a much greater reduction in the thermal conductivity than that induced by the heterogeneous elements doping or substitution.

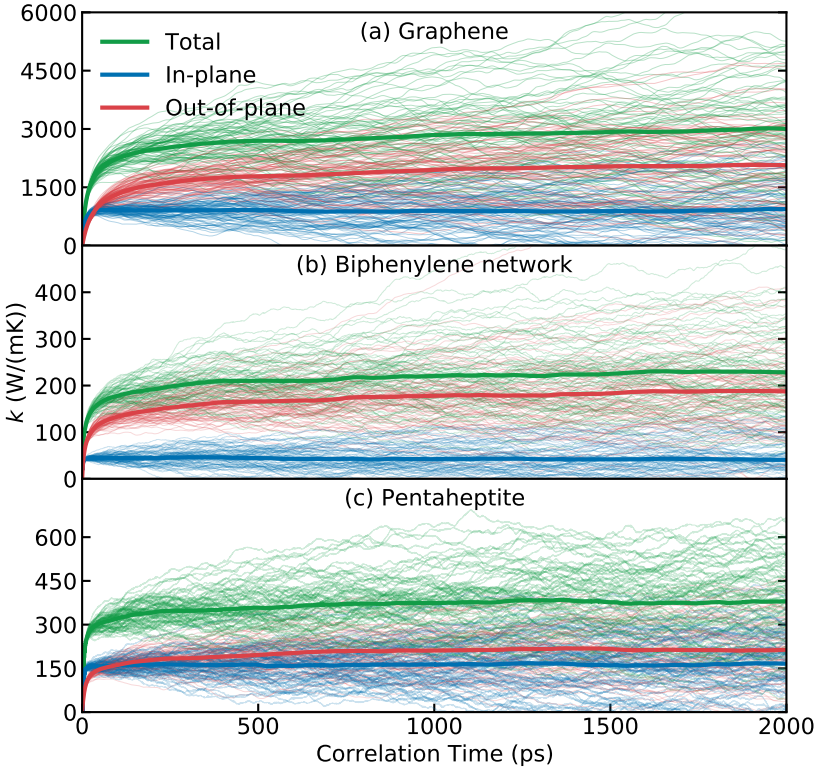


Figure 4: The thermal conductivity of (a) graphene, (b) biphenylene network, and (c) pentahepitite with the same size of 25 nm × 25 nm, which is calculated by the EMD method at 300 K. Here, the total thermal conductivity is decomposed into an in-plane component and an out-of-plane component. Each final thermal conductivity (see solid lines) is obtained by averaging by 80 independent simulations (see semi-transparent lines).

Figure 4 shows the running thermal conductivity of carbon allotropes as a function of correlation time obtained by EMD simulations. The values of $k$ obtained from EMD simulations are 2960.3 ± 301.0 W/(mK), 229.3 ±

Table 1: Thermal conductivity (in the unit of W/(mK)) of planar carbon allotropes predicted by HNEMD and EMD methods at room temperature of 300 K.

| Methods | Samples | $k_{arm}$ | $k_{zig}$ | $k_{in}$ | $k_{out}$ | $k$ |
|---|---|---|---|---|---|---|
| HNEMD | Graphene | 2807.3 | 2817.5 | 805.5 | 2007.0 | 2812.4 |
| | Biphenylene network | 213.1 | 203.5 | 38.1 | 170.2 | 208.3 |
| | Pentaheptite | 362.9 | 322.4 | 142.8 | 199.9 | 342.7 |
| EMD | Graphene | 3067.4 | 2853.2 | 904.1 | 2056.2 | 2960.3 |
| | Biphenylene network | 232.3 | 226.3 | 42.0 | 187.3 | 229.3 |
| | Pentaheptite | 398.9 | 352.4 | 162.9 | 212.8 | 375.7 |

20.5 W/(mK), and 375.7 ± 29.0 W/(mK) for graphene, biphenylene network, and pentaheptite, respectively, which are in a good agreement with the corresponding HNEMD results of 2812 ± 14.5 W/(mK), 208.3 W/(mK) ± 5.0 W/(mK), and 342.7 ± 11.3 W/(mK). Comparing the thermal conductivity components including $k_{in}$, $k_{out}$, $k_{arm}$, and $k_{zig}$ obtained from EMD and HNEMD simulations (see Table 1), we can find that both EMD and HNEMD simulations present the similar results about the anisotropy of thermal conductivity and the contribution of phonon modes. Although the production time of 1600 ns in EMD simulations is more than one order of magnitude longer than 80 ns in HNEMD simulations, the standard error of EMD results is much larger than that of their HNEMD counterparts. This divergence reveals that the statistical accuracy of the EMD is far inferior to the HNEMD, which is consistent with the conclusions extracted from previous EMD and HNEMD studies on graphene [21], carbon nanotube [21], and $C_3N$ [52].

The size effect in the NEMD method arises from the phonon scattering at the hot and cold thermostats, which leads to a length-dependent thermal conductivity $k(L)$ of the studied materials under the ballistic transport [63] at a small effective length $L$ shorter than MFP. $k$ of carbon allotropes with different $L$ is graphically shown in Fig. 5(b). As defined above, here $k$ is calculated as the average values of $k_{arm}$ and $k_{zig}$. As shown Fig. 5(b), $k$ of all carbon allotropes increases gradually with increasing $L$. Among all carbon allotropes considered here, graphene is found to have the largest growth rate. For example, when $L$ = 25 nm, $k$ of graphene is 179.4 W/(mK), which is

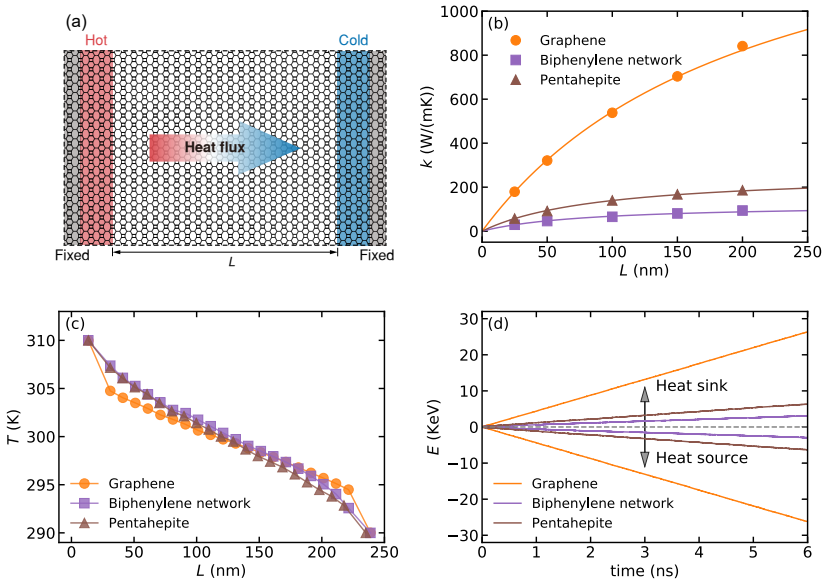


Figure 5: The thermal conductivity of three carbon allotropes calculated by NEMD method at 300 K. (a) A schematic for the setup of NEMD simulations. (b) The length-dependent thermal conductivity $k$ of the carbon allotropes with an effective length $L$ ranging from 25 nm to 500 nm. The circle and lines are results obtained from NEMD simulations and fitted by Eq.(5), respectively. (c) Temperature profile and (d) accumulated energy history in the armchair direction of three carbon allotropes with the same effective length of 200 nm.

about 6 times of the value (29.3 W/(mK)) of biphenylene network and 3 times of the value (57.5 W/(mK)) of pentaheptite. However, $k$ of graphene with $L = 200$ nm is 841.3 W/(mK), which is about 8 times and 3.5 times larger than $k$ of biphenylene network (93.9 W/(mK)) and pentaheptite (186.0 W/(mK)) with the same length, respectively. Meanwhile, it is observed that $k$ of all carbon allotropes can be well fitted by Eq.(8), indicating that the thermal transport in all carbon allotropes now exhibits the feature of ballistic transport.

In Fig. 5(c), we show a representative temperature profile along the armchair direction of the carbon allotropes with an effective length of 200 nm. The corresponding accumulated energy evolution in the thermostats of carbon allotropes is shown in Fig. 5(d). From the temperature profile, we find a dramatic temperature drop occurring near the heat source and sink of graphene, which is attributes to the more intensive phonon scattering in

graphene when compared to biphenylene network and pentaheptite. This finding is consistent with the more significant length-dependent phenomenon observed in the thermal conductivity of graphene as shown in Fig. 5(b). After applying the linear curve fitting to the accumulated energy evolution curves, we obtain the energy transfer rate of graphene, biphenylene network, and pentaheptite as 4.38 eV/ps, 0.49 eV/ps, and 1.03 eV/ps, respectively, which are consistent with the magnitudes of their thermal conductivity. In addition, through comparing $k_{arm}$ and $k_{zig}$ extracted from NEMD simulations, we also investigate the anisotropy of thermal transport in finite-size carbon allotropes as shown in Fig. S3 (see Supplementary Materials). It is observed that $k_{arm}$ is very close to $k_{zig}$ in graphene and biphenylene network, indicating an isotropic thermal transport property of these materials. As for pentaheptite, the difference between $k_{arm}$ and $k_{zig}$ is found to increase as $L$ grows. In other words, the anisotropy of thermal transport in pentaheptite will become more significant with increasing $L$, which is consistent with the HNMED and NEMD results listed in Table 1.

### *3.2. Phonon Property Analysis*

According to the classical phonon-gas model, the thermal conductivity of a crystal can be expressed as

$$k = \frac{1}{3} C_V v_g \lambda, \tag{10}$$

where $C_V$, $v_g$, and $\lambda$ are the volumetric heat capacity, phonon group velocity, and phonon MFP, respectively. From our results, it can be clearly found that the thermal transport property of both biphenylene network and pentaheptite is much weaker than that of graphene. In this section, the analysis of phonon properties including the group velocity and MFP shown in Eq. (10) is performed to reveal the origin of the difference observed in the thermal conductivity of three carbon allotropes. Specifically, the frequency-dependent MFP is obtained by SHC calculations based on HNEMD and NEMD results, while the group velocity is calculated by lattice dynamics methods. In addition, the vibrational density of states (VDOS) is also calculated to provide more information on the vibrational modes of carbon allotropes. Noted that all calculated phonon properties are based on the optimized Tersoff force field, which is consistent with the thermal conductivity calculations.

In Fig. 6, we show SHC results including spectral thermal conductivity $k(\omega)$, spectral ballistic thermal conductance $G(\omega)$, frequency-dependent

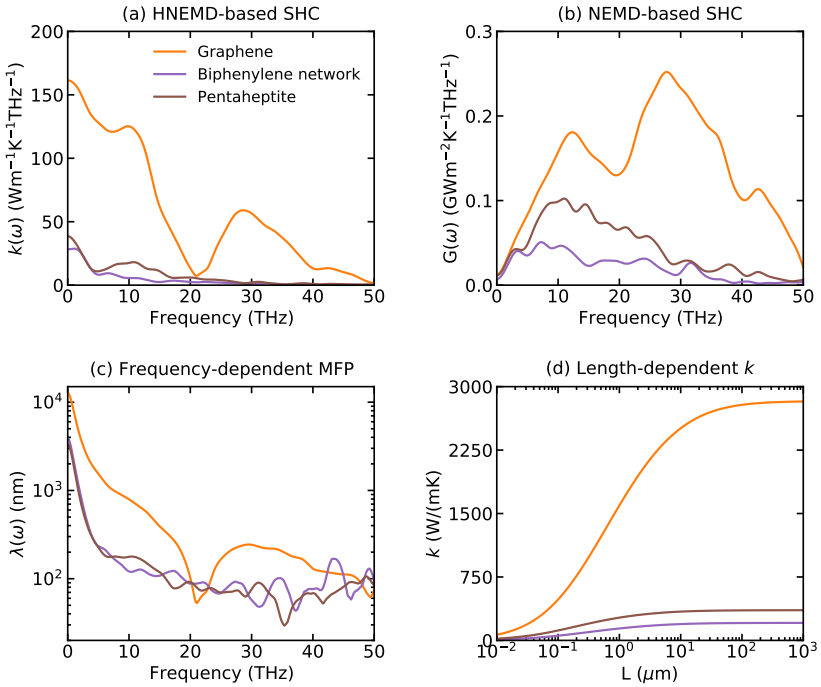


Figure 6: A comparison of SHC results of three carbon allotropes at 300 K. (a) The spectral thermal conductivity $k(\omega)$ based on HNEMD results. (b) The spectral ballistic thermal conductance $G(\omega)$ based on NEMD results. (c) The frequency-dependent MFP $\lambda(\omega)$ obtained by Eq. 7. (d) The length-dependent thermal conductivity $k$ obtained by Eq. 9.

MFP $\lambda(\omega)$, and length-dependent thermal conductivity $k(L)$ of three carbon allotropes. The corresponding in-plane and out-of-plane components of these SHC results are shown in Figs. S4 and S5 for each carbon allotrope. Here, all SHC results were obtained by averaging in armchair and zigzag directions. The result of $k$ based on HNEMD is graphically shown in Figs. 6(a) as a function of $\omega$. From this figure, we can see that $k$ of all carbon allotropes is mainly attributed to the phonon modes less than 20 THz, which is especially significant in the biphenylene network and pentaheptite. As shown in Fig. S4 (see Supplementary Materials), $k$ of graphene and pentaheptite is mainly induced by the out-of-plane modes. As for the bipheneylene network, its $k$ even almost entirely origins from the out-of-plane phonon modes. This finding is consistent with the previous HNEMD and EMD results that the out-of-plane phonon modes of biphenylene network contribute about four-fives of its ther-

mal conductivity, which is significantly larger than two-thirds contributed by out-of-plane phonon modes in both graphene and pentaheptite. After combined with $G(\omega)$ obtained by NEMD-based SHC (see Fig. 6(b)), the spectral phonon MFP $\lambda(\omega)$ can be obtained by Eq. (7), which is shown in Fig. 6(c). It is found that at extreme condition that $\omega \to 0$, the values of $\lambda_{max}$ of graphene, biphenylene network, and pentaheptite are around 10000 nm, 4000 nm, and 4000 nm, respectively. With a choice of $F_e = 0.1$ $\mu$m$^{-1}$ in HNEMD simulations, $\lambda_{max}$ is in accordance with the criteria $F_e\lambda_{max} \lesssim 1$, which further ensures that HNEMD simulations are now in the linear response region [21]. It is also clearly observed that $\lambda$ of graphene is much larger than that of biphenylene and pentaheptite at a low frequency smaller than 20 THz, which is consistent with the fact that graphene possesses the largest thermal conductivity among three carbon allotropes.

Ultimately, $k(L)$ obtained by first-order classical extrapolation (see Eqs. (8) and (9) shows that $k$ of graphene, biphenylene, and pentaheptite converges to 2785.1 W/(mK), 210.0 W/(mK), and 386.0 W/(mK), respectively, when $L$ is approaching 1 mm (see Fig. 6(d)), which agree well with our previous HNEMD and EMD results (see Table. 1). The minimum length corresponding to the onset of the convergence of $k$ is in the scale of millimeter, which indicates that the NEMD is a computationally expensive method in obtaining a convergence value of $k$ for 2D carbon allotropes. Based on NEMD simulations together with the extrapolation method, in the previous study [28], 2272.0 W/(mK) and 156.5 W/(mK) were, respectively, predicted for $k$ of graphene and biphenylene network, which are much smaller than 2812.4 W/(mK) and 208.3 W/(mK) obtained by our HNEMD method here. This large gap observed in the results obtained from the present and previous studies can be mainly attributed to the fact that the length smaller than 100 nm used in the previous study is too short to predict a reliable thermal conductivity in the extrapolation method. In addition, as shown in Fig. S5 (see Supplementary Materials), the out-of-plane phonon modes are found to contribute the major part of $\lambda(\omega)$ and $k(L)$ in all carbon allotropes, which is consistent with the the results extracted from the above $k(\omega)$.

To better understand the thermal transport in carbon allotropes considered in this study, the VDOS is calculated by performing the following Fourier integral transform on the atomic velocity auto-correlation function

(VACF) [73]:

$$\mathrm{VDOS}(\omega) = \int \langle \sum_j v_j(0) \cdot v_j(t) \rangle e^{-2\pi i \omega t} dt, \tag{11}$$

where $\sigma$ is the frequency, $i$ is the imaginary unit, and $\langle \sum_j v_j(0) \cdot v_j(t) \rangle$ is the VACF. Here, $v_j(0)$ and $v_j(t)$ are velocities of the $j$th atom at time $t$ and the initial time, respectively. Considering the planar feature of carbon allotropes considered here, their VDOS is further decomposed into three components, respectively, in armchair, zigzag, and out-of-plane directions.

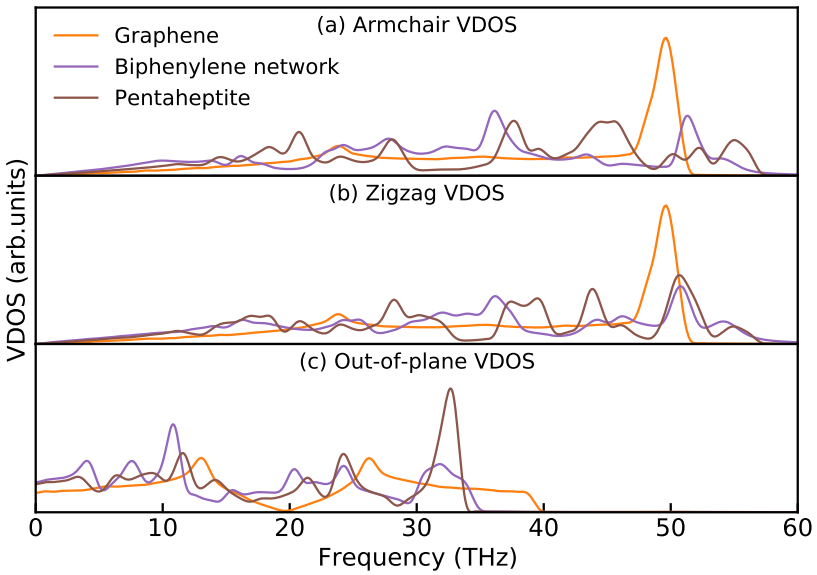


Figure 7: A comparison of VDOS of graphene, biphenylene network, and pentaheptite. Three components including (a) armchair VDOS, (b) zigzag VDOS, and (c) out-of-plane VDOS are considered here.

The armchair, zigzag, and out-of-plane components of VDOS in three carbon allotropes are shown in Fig. 7. As for all VDOS components, more modes and peaks are observed in biphenylene network and pentaheptite when compared with graphene. This difference is attributed to the fact that more atoms exist in the Bravais lattice of biphenylene network and pentaheptite, because the symmetry is greatly reduced after the structural transformation of biphenylene network and pentaheptite from graphene (see Fig. 1). As for the armchair and zigzag components of VDOS, the sharp peak around the

high frequency of 50 THz in graphene disappears in the result of biphenylene network. Based on the aforementioned SHC results, it is found that the thermal conductivity of carbon allotropes is mainly attributed to the out-of-plane phonon modes with a low frequency smaller than 20 THz. In the out-of-plane VDOS with the frequency smaller than 20 THz (see Fig. 7(c), the peaks of both biphenylene network and pentaheptite locate in the frequency region lower than that of graphene. In addition, the out-of-plane phonon VDOS in this region of biphenylene network and pentaheptite show more peaks (corresponding to more phonon modes) when compared wit the corresponding result of graphene. This difference observed in the out-of-plane VDOS of biphenylene network and pentaheptite indicates a stronger phonon scattering effect and correspondingly a shorter phonon lifetime in biphenylene network and pentaheptite, which is a factor responsible for the much weaker thermal transport property observed in biphenylene network and pentaheptite when compared with that of graphene. A further comparison among the armchair VDOS, zigzag VDOS, and out-of-plane VDOS of each carbon allotrope is shown in Fig. S6 (see supplementary materials). It is found that the armchair VDOS and zigzag VDOS in graphene are identical to each other very well. Simialrly, the armchair VDOS in biphenylene network the is very close to the zigzag VDOS. However, the armchair VDOS in pentaheptite is clearly found to be different with its zigzag VDOS, which is consistent with its anisotropic thermal transport property as shown in Table 1.

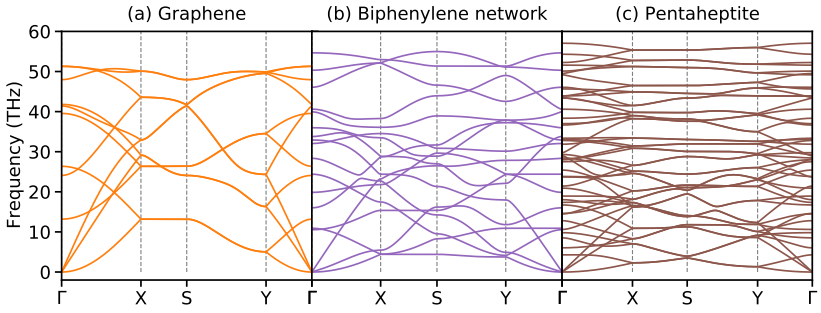


Figure 8: The phonon dispersion curves of (a) graphene, (b) biphenylene network, and (c) pentaheptite along high symmetry directions of the first Brillouin zone.

The aforementioned SHC analysis suggests that the phonon MFP of graphene is much longer than that of two other carbon allotropes, which

is an important factor responsible for the much higher thermal conductivity observed in graphene. In addition to the phonon MFP, as suggested by the classical phonon-gas model in Eq. 10, the phonon group velocity is another important parameter determining the lattice thermal conductivity. Thus, we show the phonon dispersion curves of three carbon allotropes obtained by lattice dynamics calculations in Fig. 8 and further compare their phonon group velocities in Fig. 9. For the sake of comparison, the high symmetry direction of the first Brillouin zone is set as $\Gamma - \mathrm{X} - \mathrm{S} - \mathrm{Y} - \Gamma$ for all carbon allotropes (see Figs. S1 and 8). Among three acoustic modes, the longitudinal acoustic (LA) and transverse acoustic (TA) modes of all carbon allotropes show linear dispersion, while their flexural out-of-plane acoustic (ZA) mode shows a quadratic dispersion, which is a classical characteristic of phonon dispersion curves of monolayer 2D materials [34]. It is found that the frequency corresponding to the acoustic modes of graphene locates much higher than that of biphenylene network and pentaheptite. For example, at the X point, frequencies at LA, TA, and ZA modes of graphene are, respectively, around 33 THz, 26 THz, and 13 THz, which are much larger than the corresponding results of biphenylene network (24 THz, 6 THz, and 4 THz) and pentaheptite (16 THz, 11 THz, and 2 THz). The speed of sound equaling to the slope of all three acoustic modes in biphenylene network and pentaheptite is found to be much smaller than that in graphene. This difference is directly related to the different group velocities observed among three carbon allotropes as shown in Fig. 9.

From Fig. 9, it can be obviously observed that the average group velocity of biphenylene network and pentaheptite is significantly smaller than that of graphene at low frequency region smaller than 20 THz, which mainly contributes to the thermal conductivity. The highest value of average group velocity is found to decrease from 12.0 km/s of graphene to 8.9 km/s of biphenylene network and 9.1 km/s of pentaheptite, which indicates a weaker phonon transport property and correspondingly a much lower thermal conductivity of biphenylene network and pentaheptite compared to that of graphene. Although biphenylene network and pentaheptite have almost the same highest value of average group velocity, the group velocity of biphenylene network within the low frequency smaller than 15 THz is much smaller than that of pentaheptite, leading to a thermal conductivity of 208.3 W/(mK) of biphenylene network that is much smaller than 342.7 W/(mK) of pentaheptite.

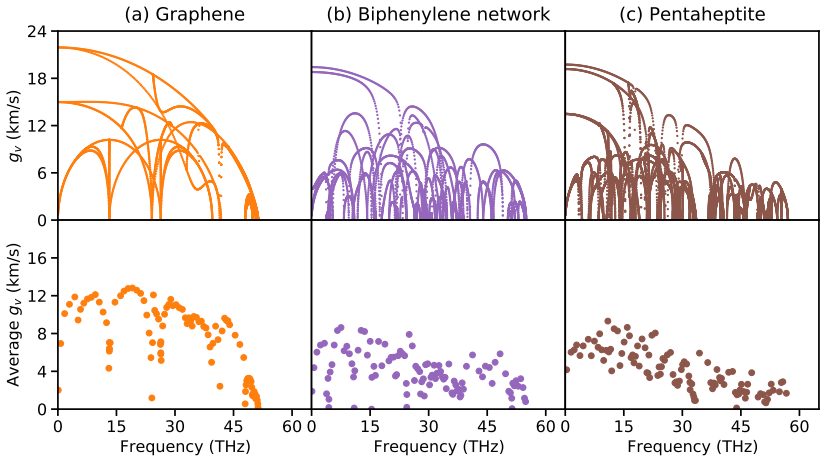


Figure 9: A comparison of the phonon group velocity $g_v$ and the corresponding average group velocity of (a) graphene, (b) biphenylene network, and (c) pentaheptite. The averaged $g_v$ is obtained by averaging the group velocity each 1 THz.

### *3.3. Electron Density and Mechanical Properties*

In the above discussion, we have demonstrated that the phonon MFP and group velocity of biphenylene network and pentaheptite are significantly smaller than those of graphene, which is responsible for the much weaker thermal transport property observed in biphenylene network and pentaheptite. Furthermore, although the phonon MFP of biphenylene network is close to that of pentaheptite, the biphenylene network has a group velocity smaller than that of pentaheptite. Thus, among three carbon allotropes, the lowest thermal conductivity is observed in biphenylene network. To reveal the origin of the significant reduction in phonon MFP and group velocity of biphenylene network and pentaheptite, the electron localization function (ELF) [74] of all carbon allotropes is graphically plotted in Fig. 10(a) to illustrate their atomic bonding features. It is found that the electron localization occurs around the center of all bonds in three carbon allotropes, which, as expected, clearly indicates the dominance of covalent bonding. However, the electron localization of biphenylene network prefers to locate in the space of eight-membered and six-membered rings and deviates from the four-membered rings. A similar distribution is also found in pentaheptite, in which the electron localization prefers to locate in the seven-membered rings rather than five-membered rings. The deviation degree of electron localization in biphenylene is greater than that in pentaheptite, while no deviation is found in graphene due to its

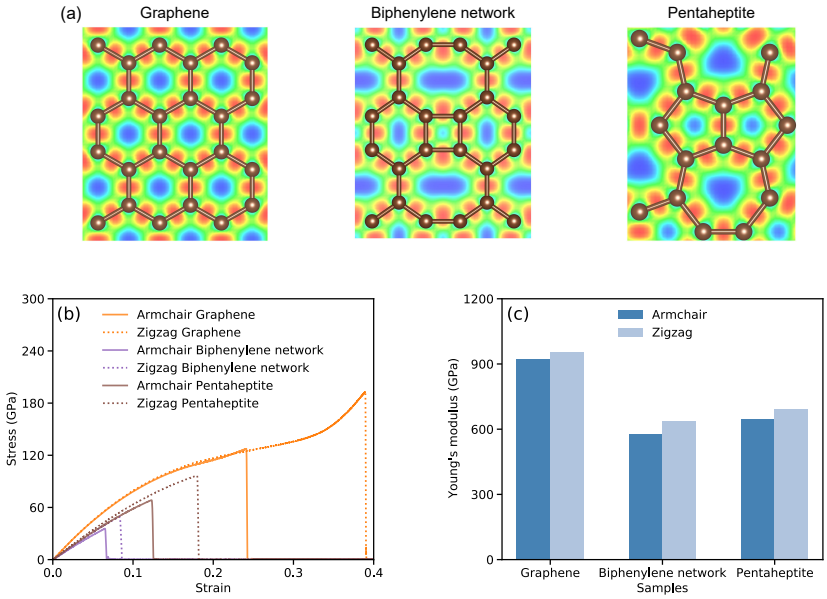


Figure 10: (a) The ELF of graphene, biphenylene network, and pentaheptite. (b) Stress-strain response of graphene, biphenylene network, and pentaheptite uniaxially elongated along armchair and zigzag directions. (c) The corresponding Young's modulus obtained from tensile simulations.

perfect symmetry structure with six-membered rings. This can be explained by the difference in structural symmetry of studied carbon allotropes. For example, the inner space of four-membered rings in biphenylene is much smaller than that of its six-membered and eight-membered rings. As a result, the electron localization moves to the six-membered and eight-membered rings due to the repulsion force between electrons in a small space. The similar mechanism is also applicable for the five-membered and seven-membered rings in pentaheptite.

The deviation of electronic localization in biphenylene network and pentaheptite reveals that their bond property is different to that of graphene at the electronic scale. We further performed the MD simulations of uniaxial tensile test on three carbon allotropes to compare their mechanical properties (see supplementary materials for corresponding simulation details). Fig 10(b) shows the stress-strain curves of three carbon allotropes along armchair and zigzag directions. The corresponding Young's modulus was obtained through performing the linear curve fitting to the stress-strain curves with the strain

smaller than 0.04. Among these carbon allotropes, graphene is found to possess the largest strength and Young's modulus, followed by pentaheptite and biphenylene network. This trend is consistent with their thermal conductivity. The Young's moduli of graphene, biphenylene network, and pentaheptite in the armchair direction are 924.4 GPa, 576.8 GPa and 644.9 GPa, respectively, while their values in the zigzag direction are 954.7 GPa, 637.1 GPa and 694.0 GPa, respectively (see Fig 10(c)). Based on the ELF analysis together with calculated mechanical properties of various carbon allotropes, we can see that due to the reduction in the structural symmetry of biphenylene network and pentaheptite, their bond property and mechanical properties are different from those of graphene, which leads to the stronger phonon scattering and correspondingly the lower phonon group velocity and MFP observed in biphenylene network and pentaheptite. These differences finally result in the weaker phonon transport property observed in biphenylene network and pentaheptite.

## 4. Conclusion

In conclusion, the thermal transport in three planar $sp^2$-hybridized carbon allotropes including graphene, biphenylene network, and pentaheptite is investigated in this study by MD simulations together first-principles calculations. Three MD-based methods, i.e., HNEMD, EMD, and NEMD are employed to obtain a reliable prediction of the thermal conductivity of these carbon allotropes. According to our HNEMD results, the thermal conductivities of biphenylene network and pentaheptite are 208.3 W/(mK) and 342.7 W/(mK), respectively, which are only one-thirteenth and one-eighth of the value (2812.4 W/(mK)) of graphene. The much smaller thermal conductivity observed in biphenylene network and pentaheptite originates from the symmetry breaking of the pristine honeycomb lattice during the structural transformation from graphene to biphenylene network and pentaheptite. The results obtained from EMD and NEMD simulations are in good agreement with those from HNEMD simulations, which, to some extent, proves the reliability of the results predicted from the present calculations. In addition, it is also found that the thermal conductivity of all three carbon allotropes is mainly attributed to the flexural phonon modes. Especially for biphenylene network, the flexural phonon contributes up to four-fifths of the total thermal conductivity. The SHC analysis and lattice dynamics analysis demonstrate that both the phonon group velocity and mean MFP of biphenylene network

and pentaheptite are much smaller than those of graphene. Furthermore, the deviation of ELF found in biphenylene network and pentaheptite indicates different bond properties existing in these two carbon allotropes and graphene, which results in a larger anharmonicity and stronger phonon scattering in them when compared those of graphene. This mechanism is further proved through the different mechanical properties observed among these carbon allotropes. Our study not only provides a deep understanding on fundamental mechanisms of phonon transport in 2D carbon allotropes, but also facilitate their applications in carbon nanodevices.

## References


[1] K. S. Novoselov, A. K. Geim, S. V. Morozov, D. Jiang, Y. Zhang, S. V. Dubonos, I. V. Grigorieva, A. A. Firsov, Electric field effect in atomically thin carbon films, science 306 (5696) (2004) 666–669.

[2] C. Lee, X. Wei, J. W. Kysar, J. Hone, Measurement of the elastic properties and intrinsic strength of monolayer graphene, science 321 (5887) (2008) 385–388.

[3] A. A. Balandin, S. Ghosh, W. Bao, I. Calizo, D. Teweldebrhan, F. Miao, C. N. Lau, Superior thermal conductivity of single-layer graphene, Nano letters 8 (3) (2008) 902–907.

[4] W. Cai, A. L. Moore, Y. Zhu, X. Li, S. Chen, L. Shi, R. S. Ruoff, Thermal transport in suspended and supported monolayer graphene grown by chemical vapor deposition, Nano letters 10 (5) (2010) 1645–1651.

[5] S. Ghosh, W. Bao, D. L. Nika, S. Subrina, E. P. Pokatilov, C. N. Lau, A. A. Balandin, Dimensional crossover of thermal transport in few-layer graphene, Nature materials 9 (7) (2010) 555–558.

[6] S. Chen, A. L. Moore, W. Cai, J. W. Suk, J. An, C. Mishra, C. Amos, C. W. Magnuson, J. Kang, L. Shi, et al., Raman measurements of thermal transport in suspended monolayer graphene of variable sizes in vacuum and gaseous environments, ACS nano 5 (1) (2011) 321–328.

[7] G. R. Bhimanapati, Z. Lin, V. Meunier, Y. Jung, J. Cha, S. Das, D. Xiao, Y. Son, M. S. Strano, V. R. Cooper, et al., Recent advances in two-dimensional materials beyond graphene, ACS nano 9 (12) (2015) 11509–11539.

[8] R. Van Noorden, Moving towards a graphene world (2006).

[9] A. Balaban, C. C. Rentia, E. Ciupitu, Chemical graphs. 6. estimation of relative stability of several planar and tridimensional lattices for elementary carbon, Revue Roumaine de Chimie 13 (2) (1968) 231–+.

[10] V. H. Crespi, L. X. Benedict, M. L. Cohen, S. G. Louie, Prediction of a pure-carbon planar covalent metal, Physical Review B 53 (20) (1996) R13303.

[11] A. N. Enyashin, A. L. Ivanovskii, Graphene allotropes, physica status solidi (b) 248 (8) (2011) 1879–1883.

[12] Y. Liu, G. Wang, Q. Huang, L. Guo, X. Chen, Structural and electronic properties of t graphene: a two-dimensional carbon allotrope with tetrarings, Physical review letters 108 (22) (2012) 225505.

[13] L.-C. Xu, R.-Z. Wang, M.-S. Miao, X.-L. Wei, Y.-P. Chen, H. Yan, W.-M. Lau, L.-M. Liu, Y.-M. Ma, Two dimensional dirac carbon allotropes from graphene, Nanoscale 6 (2) (2014) 1113–1118.

[14] Z. Wang, X.-F. Zhou, X. Zhang, Q. Zhu, H. Dong, M. Zhao, A. R. Oganov, Phagraphene: a low-energy graphene allotrope composed of 5–6–7 carbon rings with distorted dirac cones, Nano letters 15 (9) (2015) 6182–6186.

[15] Z. Gong, X. Shi, J. Li, S. Li, C. He, T. Ouyang, C. Zhang, C. Tang, J. Zhong, Theoretical prediction of low-energy stone-wales graphene with an intrinsic type-iii dirac cone, Physical Review B 101 (15) (2020) 155427.

[16] J.-W. Jiang, J. Leng, J. Li, Z. Guo, T. Chang, X. Guo, T. Zhang, Twin graphene: A novel two-dimensional semiconducting carbon allotrope, Carbon 118 (2017) 370–375.

[17] G. Li, Y. Li, H. Liu, Y. Guo, Y. Li, D. Zhu, Architecture of graphdiyne nanoscale films, Chemical Communications 46 (19) (2010) 3256–3258.

[18] K. Sääskilahti, J. Oksanen, J. Tulkki, S. Volz, Role of anharmonic phonon scattering in the spectrally decomposed thermal conductance at planar interfaces, Physical Review B 90 (13) (2014) 134312.

[19] M. Liu, M. Liu, L. She, Z. Zha, J. Pan, S. Li, T. Li, Y. He, Z. Cai, J. Wang, et al., Graphene-like nanoribbons periodically embedded with four-and eight-membered rings, Nature communications 8 (1) (2017) 1–7.

[20] Q. Fan, L. Yan, M. W. Tripp, O. Krejčí, S. Dimosthenous, S. R. Kachel, M. Chen, A. S. Foster, U. Koert, P. Liljeroth, et al., Biphenylene network: A nonbenzenoid carbon allotrope, Science 372 (6544) (2021) 852–856.

[21] Z. Fan, H. Dong, A. Harju, T. Ala-Nissila, Homogeneous nonequilibrium molecular dynamics method for heat transport and spectral decomposition with many-body potentials, Physical Review B 99 (6) (2019) 064308.

[22] X. Yang, Z. Dai, Y. Zhao, S. Meng, Phonon thermal transport in a class of graphene allotropes from first principles, Physical Chemistry Chemical Physics 20 (23) (2018) 15980–15985.

[23] S. Zhang, J. Zhou, Q. Wang, X. Chen, Y. Kawazoe, P. Jena, Penta-graphene: A new carbon allotrope, Proceedings of the National Academy of Sciences 112 (8) (2015) 2372–2377.

[24] F. Q. Wang, J. Yu, Q. Wang, Y. Kawazoe, P. Jena, Lattice thermal conductivity of penta-graphene, Carbon 105 (2016) 424–429.

[25] M. S. Green, Markoff random processes and the statistical mechanics of time-dependent phenomena. ii. irreversible processes in fluids, The Journal of Chemical Physics 22 (3) (1954) 398–413.

[26] R. Kubo, Statistical-mechanical theory of irreversible processes. i. general theory and simple applications to magnetic and conduction problems, Journal of the Physical Society of Japan 12 (6) (1957) 570–586.

[27] C. Su, H. Jiang, J. Feng, Two-dimensional carbon allotrope with strong electronic anisotropy, Physical Review B 87 (7) (2013) 075453.

[28] H. Dong, Z. Zhang, Z. Feng, J. Kang, D. Wu, Q. Wang, J. Li, R. Su, Origins of low lattice thermal conductivity in 2d carbon allotropes, Journal of Materials Research and Technology 11 (2021) 1982–1990.

[29] X. Li, Q. Wang, P. Jena, $\psi$-graphene: a new metallic allotrope of planar carbon with potential applications as anode materials for lithium-ion batteries, The journal of physical chemistry letters 8 (14) (2017) 3234–3241.

[30] S. Wang, B. Yang, H. Chen, E. Ruckenstein, Popgraphene: a new 2d planar carbon allotrope composed of 5–8–5 carbon rings for high-performance lithium-ion battery anodes from bottom-up programming, Journal of Materials Chemistry A 6 (16) (2018) 6815–6821.

[31] L. Lindsay, D. Broido, N. Mingo, Flexural phonons and thermal transport in graphene, Physical Review B 82 (11) (2010) 115427.

[32] Z. Fan, L. F. C. Pereira, P. Hirvonen, M. M. Ervasti, K. R. Elder, D. Donadio, T. Ala-Nissila, A. Harju, Thermal conductivity decomposition in two-dimensional materials: Application to graphene, Physical Review B 95 (14) (2017) 144309.

[33] D. L. Nika, A. A. Balandin, Phonons and thermal transport in graphene and graphene-based materials, Reports on Progress in Physics 80 (3) (2017) 036502.

[34] X. Gu, Z. Fan, H. Bao, C. Zhao, Revisiting phonon-phonon scattering in single-layer graphene, Physical Review B 100 (6) (2019) 064306.

[35] N. Wei, S. Li, Y. Zhang, J. Chen, Y. Chen, J. Zhao, Thermal rectification of graphene on substrates with inhomogeneous stiffness, Carbon 154 (2019) 81–89.

[36] Z. Fan, T. Siro, A. Harju, Accelerated molecular dynamics force evaluation on graphics processing units for thermal conductivity calculations, Computer Physics Communications 184 (5) (2013) 1414–1425.

[37] W. C. Swope, H. C. Andersen, P. H. Berens, K. R. Wilson, A computer simulation method for the calculation of equilibrium constants for the formation of physical clusters of molecules: Application to small water clusters, The Journal of chemical physics 76 (1) (1982) 637–649.

[38] S. Plimpton, Fast parallel algorithms for short-range molecular dynamics, Journal of computational physics 117 (1) (1995) 1–19.

[39] Z. Fan, L. F. C. Pereira, H.-Q. Wang, J.-C. Zheng, D. Donadio, A. Harju, Force and heat current formulas for many-body potentials in molecular dynamics simulations with applications to thermal conductivity calculations, Physical Review B 92 (9) (2015) 094301.

[40] P. Boone, H. Babaei, C. E. Wilmer, Heat flux for many-body interactions: corrections to lammps, Journal of chemical theory and computation 15 (10) (2019) 5579–5587.

[41] P. Ying, J. Zhang, X. Zhang, Z. Zhong, Impacts of functional group substitution and pressure on the thermal conductivity of zif-8, The Journal of Physical Chemistry C 124 (11) (2020) 6274–6283.

[42] L. Lindsay, D. Broido, Optimized tersoff and brenner empirical potential parameters for lattice dynamics and phonon thermal transport in carbon nanotubes and graphene, Physical Review B 81 (20) (2010) 205441.

[43] Z. G. Fthenakis, Z. Zhu, D. Tomanek, Effect of structural defects on the thermal conductivity of graphene: from point to line defects to haeckelites, Physical Review B 89 (12) (2014) 125421.

[44] K. Azizi, P. Hirvonen, Z. Fan, A. Harju, K. R. Elder, T. Ala-Nissila, S. M. V. Allaei, Kapitza thermal resistance across individual grain boundaries in graphene, Carbon 125 (2017) 384–390.

[45] B. Mortazavi, O. Rahaman, T. Rabczuk, L. F. C. Pereira, Thermal conductivity and mechanical properties of nitrogenated holey graphene, Carbon 106 (2016) 1–8.

[46] Z. Li, S. Xiong, C. Sievers, Y. Hu, Z. Fan, N. Wei, H. Bao, S. Chen, D. Donadio, T. Ala-Nissila, Influence of thermostatting on nonequilibrium molecular dynamics simulations of heat conduction in solids, The Journal of chemical physics 151 (23) (2019) 234105.

[47] W. Xu, G. Zhang, B. Li, Thermal conductivity of penta-graphene from molecular dynamics study, The Journal of chemical physics 143 (15) (2015) 154703.

[48] S. Li, H. Ren, Y. Zhang, X. Xie, K. Cai, C. Li, N. Wei, Thermal conductivity of two types of 2d carbon allotropes: A molecular dynamics study, Nanoscale research letters 14 (1) (2019) 1–11.

[49] X. Wu, Q. Han, Thermal conductivity of monolayer hexagonal boron nitride: From defective to amorphous, Computational Materials Science 184 (2020) 109938.

[50] P. Ying, J. Zhang, Y. Du, Z. Zhong, Effects of coating layers on the thermal transport in carbon nanotubes-based van der waals heterostructures, Carbon 176 (2021) 446–457.

[51] M. An, L. Li, S. Hu, Z. Ding, X. Yu, B. Demir, N. Yang, W. Ma, X. Zhang, Mass difference and polarization lead to low thermal conductivity of graphene-like carbon nitride (c3n), Carbon 162 (2020) 202–208.

[52] X. Wu, Q. Han, Thermal transport in pristine and defective two-dimensional polyaniline (c3n), International Journal of Heat and Mass Transfer 173 (2021) 121235.

[53] B. Mortazavi, M. Shahrokhi, M. Raeisi, X. Zhuang, L. F. C. Pereira, T. Rabczuk, Outstanding strength, optical characteristics and thermal conductivity of graphene-like bc3 and bc6n semiconductors, Carbon 149 (2019) 733–742.

[54] S. J. Stuart, A. B. Tutein, J. A. Harrison, A reactive potential for hydrocarbons with intermolecular interactions, The Journal of chemical physics 112 (14) (2000) 6472–6486.

[55] K. Chenoweth, A. C. Van Duin, W. A. Goddard, Reaxff reactive force field for molecular dynamics simulations of hydrocarbon oxidation, The Journal of Physical Chemistry A 112 (5) (2008) 1040–1053.

[56] D. J. Evans, Homogeneous nemd algorithm for thermal conductivity—application of non-canonical linear response theory, Physics Letters A 91 (9) (1982) 457–460.

[57] H. Wang, Y. Cheng, Z. Fan, Y. Guo, Z. Zhang, M. Bescond, M. Nomura, S. Volz, T. Ala-Nissila, S. Xiong, Anomalous thermal conductivity enhancement in low dimensional resonant nanostructures due to imperfections, Nanoscale (2021).

[58] A. J. Gabourie, S. V. Suryavanshi, A. B. Farimani, E. Pop, Reduced thermal conductivity of supported and encased monolayer and bilayer mos2, 2D Materials 8 (1) (2020) 011001.

[59] Z. Yao, J.-S. Wang, B. Li, G.-R. Liu, Thermal conduction of carbon nanotubes using molecular dynamics, Physical Review B 71 (8) (2005) 085417.

[60] K. K. Mandadapu, R. E. Jones, P. Papadopoulos, A homogeneous nonequilibrium molecular dynamics method for calculating thermal conductivity with a three-body potential, The Journal of chemical physics 130 (20) (2009) 204106.

[61] B. Dongre, T. Wang, G. K. Madsen, Comparison of the green–kubo and homogeneous non-equilibrium molecular dynamics methods for calculating thermal conductivity, Modelling and Simulation in Materials Science and Engineering 25 (5) (2017) 054001.

[62] J. M. Haile, I. Johnston, A. J. Mallinckrodt, S. McKay, Molecular dynamics simulation: elementary methods, Computers in Physics 7 (6) (1993) 625–625.

[63] K. Sääskilahti, J. Oksanen, S. Volz, J. Tulkki, Frequency-dependent phonon mean free path in carbon nanotubes from nonequilibrium molecular dynamics, Physical Review B 91 (11) (2015) 115426.

[64] A. J. Gabourie, Z. Fan, T. Ala-Nissila, E. Pop, Spectral decomposition of thermal conductivity: Comparing velocity decomposition methods in homogeneous molecular dynamics simulations, Physical Review B 103 (20) (2021) 205421.

[65] P. K. Schelling, S. R. Phillpot, P. Keblinski, Comparison of atomic-level simulation methods for computing thermal conductivity, Physical Review B 65 (14) (2002) 144306.

[66] G. Kresse, J. Furthmüller, Efficiency of ab-initio total energy calculations for metals and semiconductors using a plane-wave basis set, Computational materials science 6 (1) (1996) 15–50.

[67] G. Kresse, J. Furthmüller, Efficient iterative schemes for ab initio total-energy calculations using a plane-wave basis set, Physical review B 54 (16) (1996) 11169.

[68] G. Kresse, D. Joubert, From ultrasoft pseudopotentials to the projector augmented-wave method, Physical review b 59 (3) (1999) 1758.

[69] J. P. Perdew, K. Burke, M. Ernzerhof, Generalized gradient approximation made simple, Physical review letters 77 (18) (1996) 3865.

[70] A. Togo, I. Tanaka, First principles phonon calculations in materials science, Scripta Materialia 108 (2015) 1–5.

[71] K. Momma, F. Izumi, Vesta 3 for three-dimensional visualization of crystal, volumetric and morphology data, Journal of applied crystallography 44 (6) (2011) 1272–1276.

[72] V. Wang, N. Xu, J.-C. Liu, G. Tang, W.-T. Geng, Vaspkit: a user-friendly interface facilitating high-throughput computing and analysis using vasp code, Computer Physics Communications (2021) 108033.

[73] J. Dickey, A. Paskin, Computer simulation of the lattice dynamics of solids, Physical Review 188 (3) (1969) 1407.

[74] B. Silvi, A. Savin, Classification of chemical bonds based on topological analysis of electron localization functions, Nature 371 (6499) (1994) 683–686.

# Supplementary Materials for Thermal transport in planar $sp^2$-hybridized carbon allotropes: A comparative study

Penghua Ying[a,1], Ting Liang[b,1], Yao Du[a,1], Jin Zhang[a,*], Zheng Zhong[a,*]

[a] *School of Science, Harbin Institute of Technology, Shenzhen, 518055, PR China*
[b] *Institute of Advanced Materials Science and Engineering, Shenzhen Institutes of Advanced Technology, Chinese Academy of Sciences, Shenzhen, 518055, PR China*

## S1. Supplementary Figures

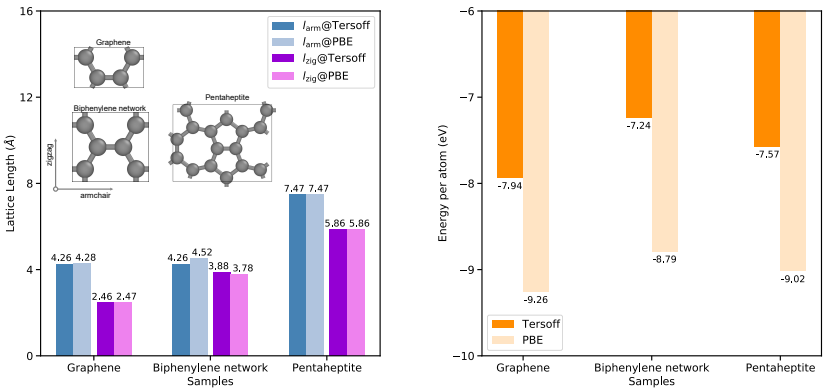


Figure S1: A comparison on the lattice length (left) and energy per atom (right) of three planar carbon allotropes predicted by classical molecular dynamics simulations at 300K with optimized Tersoff force filed (labled as "Tersoff") and first-principles calculations with Perdew-BurkeErnzerhof generalized gradient approximation for the exchange correlation potential (labled as "PBE"). $l_{\mathrm{arm}}$ and $l_{\mathrm{zig}}$ respectively represents the lattice length along armchair and zigzag directions as shown in the inset.

*Corresponding author
**Corresponding author
*Email addresses:* jinzhang@hit.edu.cn (Jin Zhang), zhongzheng@hit.edu.cn (Zheng Zhong)
[1] These authors contributed equally.

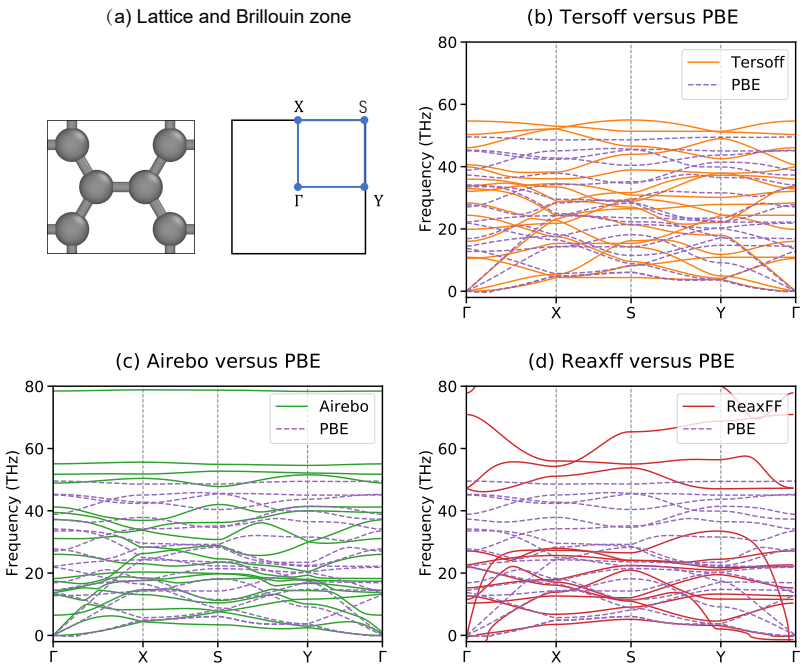


Figure S2: The phonon dispersion relations of biphenylene network predicted by classical force fields and first-principles calculations. (a) The high symmetry directions of the first Brillouin zone. (b-d) The phonon band structures predicted by first-principles calculations with PBE potential (labled as "PBE") versus optimized Tersoff force filed (labled as "Tersoff"), (c) Airebo force filed (labled as "Airebo"), and (d) ReaxFF potential (labled as "ReaxFF").

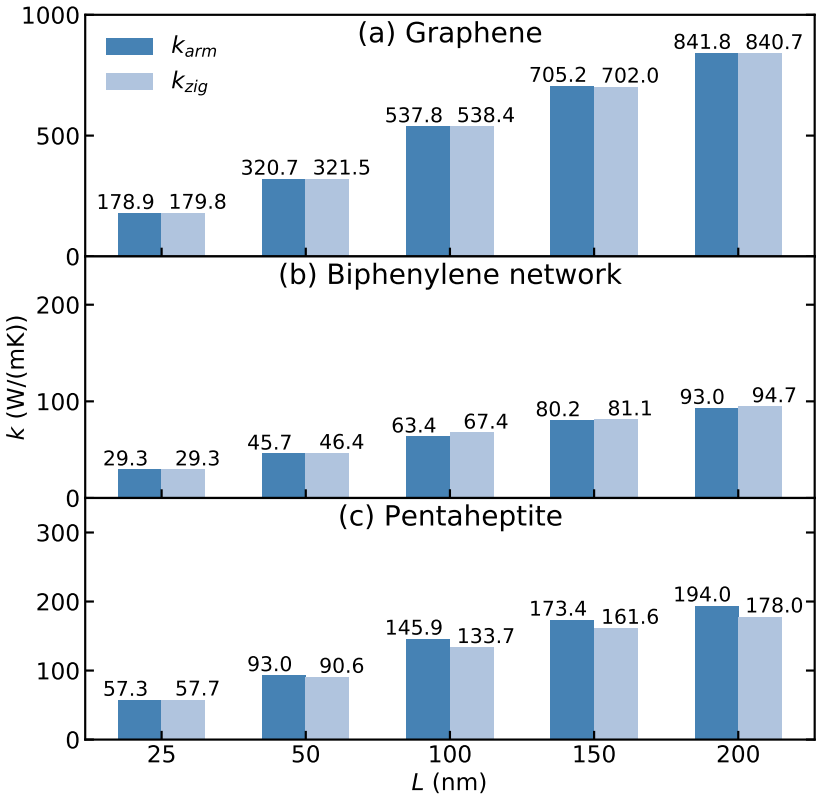


Figure S3: A comparison on the thermal conductivity along armchair direction and zigzag direction, i.e., $k_{arm}$ and $k_{zig}$ based on NEMD simulations for all carbon allotropes.

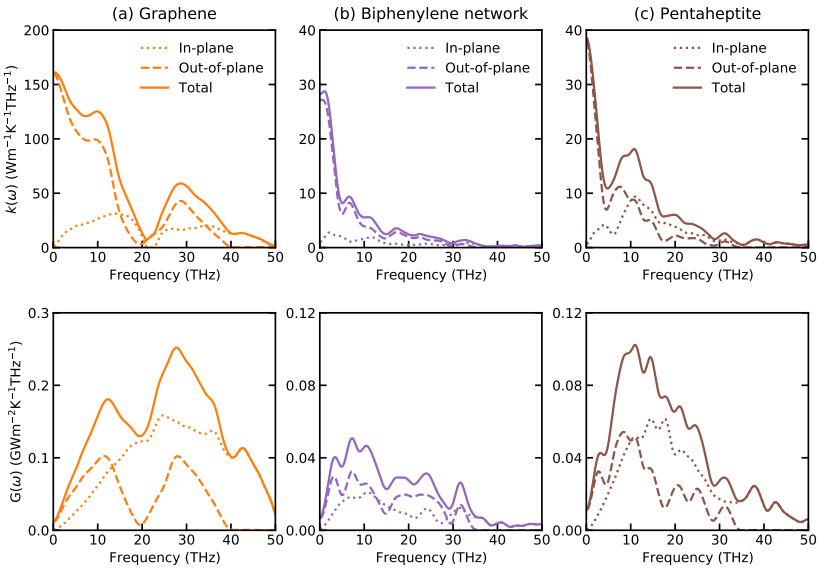


Figure S4: A comparison on the spectral thermal conductivity $k(\omega)$ (top) and ballistic thermal conductance $G(\omega)$ (bottom) contributed by in-plane and out-of-plane phonon modes for three carbon allotropes: (a) graphene, (b) biphenylene network, (c) pentaheptite. All the results are calculated at 300 K.

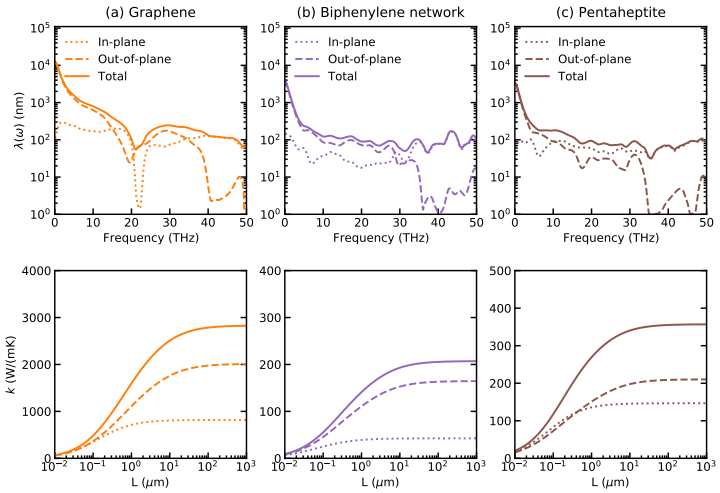


Figure S5: A comparison on the frequency-dependent MFP $\lambda(\omega)$ (top) and length-dependent thermal conductivity $k$ (bottom) contributed by in-plane and out-of-plane phonon modes for three carbon allotropes: (a) graphene, (b) biphenylene network, (c) pentaheptite. All the results are calculated at 300 K.

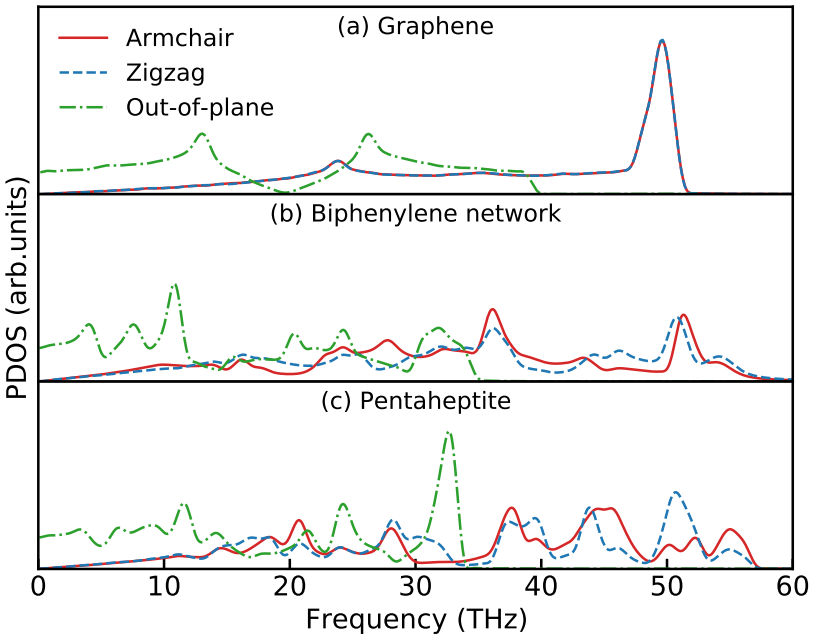


Figure S6: A comparison of armchair VDOS, zigzag VDOS, and out-of-plane VDOS for three carbon allotropes including (a) graphene, (b) biphenylene network, and (c) pentaheptite.

## S2. Supplementary Note

The tensile simulations of all carbon allotropes were performed by using large-scale atomic/molecular massively parallel simulator (LAMMPS) package [1]. A sample size of 25 nm $\times$ 25 nm was used in all tensile simulations, which is consistent with the HNEMD and EMD simulations. The thickness of all carbon allotropes was set as 0.335 nm. The periodic boundary conditions were applied in planar directions, while free boundary condiction was applied in the out-of-plane direction. Here, the optimized Tersoff potential developed by Lindsay and Broido[2] was used to simulate the C–C interaction in the carbon allotropes. The time steps in all tensile simulations were set as 1 fs. The uniaxial tensile simulations were performed at the room temperature of 300K. In doing this, an energy minimization was firstly performed using the conjugate gradient algorithm. The system was then relaxed within the isothermal-isobaric (NPT) ensemble at the temperature of 300 K and zero external pressure for 200 ps. Afterwards, the uniaxial tensile test was performed by expanding the box size in the armchair (or zigzag) direction with a strain rate of $10^9$/s while the zigzag (or armchair) direction is set as free.

## References


[S1] S. Plimpton, Fast parallel algorithms for short-range molecular dynamics, Journal of computational physics 117 (1) (1995) 1–19.

[S2] L. Lindsay, D. Broido, Optimized tersoff and brenner empirical potential parameters for lattice dynamics and phonon thermal transport in carbon nanotubes and graphene, Physical Review B 81 (20) (2010) 205441.